HHS Public Access

Author manuscript

J Clin Pharmacol. Author manuscript; available in PMC 2017 November 01.

Published in final edited form as:

J Clin Pharmacol. 2016 November ; 56(11): 1433–1447. doi:10.1002/jcph.751.

Integrating Dynamic Positron Emission Tomography and Conventional Pharmacokinetic Studies to Delineate Plasma and Tumor Pharmacokinetics of FAU, a Prodrug Bioactivated by Thymidylate Synthase

Jing Li, PhD[1,*], **Seongho Kim, PhD**[1,*], **Anthony F. Shields, MD, PhD**[1], **Kirk A. Douglas, MS**[1], **Christopher I. McHugh, BS**[1], **Jawana M. Lawhorn-Crews, BS**[1], **Jianmei Wu, PhD**[1], **Thomas J. Mangner, PhD**[2], and **Patricia M. LoRusso, DO**[3]

[1]Karmanos Cancer Institute, Department of Oncology, Wayne State University School of Medicine, Detroit, MI 48201

[2]Department of Radiology, Wayne State University, Detroit, MI, 48201

[3]Yale Cancer Center, Yale School of Medicine, New Haven, CT 06520

Abstract

FAU, a pyrimidine nucleotide analog, is a prodrug bioactivated by intracellular thymidylate synthase to form FMAU that is incorporated into DNA causing cell death. This study presents a model-based approach to integrating dynamic positron emission tomography (PET) and conventional plasma pharmacokinetic studies to characterize the plasma and tissue pharmacokinetics of FAU and FMAU. Twelve cancer patients were enrolled into a phase I study, where conventional plasma pharmacokinetic evaluation of therapeutic FAU (50 – 1600 mg/m^2) and dynamic PET assessment of ^{18}F-FAU were performed. A parent-metabolite population pharmacokinetic model was developed to simultaneously fit PET-derived tissue data and conventional plasma pharmacokinetic data. The developed model enabled separation of PET-derived total tissue concentrations into the parent drug and metabolite components. The model provides quantitative, mechanistic insights into the bioactivation of FAU and retention of FMAU in normal and tumor tissues, and has potential utility to predict tumor responsiveness to FAU treatment.

Requests for reprints: Jing Li, Ph.D., Karmanos Cancer Institute, Wayne State University School of Medicine, 4100 John R, HWCRC/Room 523, Detroit, MI, 48201; Phone: 313-576-8258; lijin@karmanos.org; or Patricia M. LoRusso, D.O., Yale Cancer Center, WWW217, 333 Cedar Street, New Haven, CT 06510; Phone: 203-785-5944; Fax: 203-785-4116.

*J Li and S Kim contributed equally to this work.

CONFLICT OF INTEREST/DISCLOSURE

The authors declare that there are no conflicts of interest.

AUTHOR CONTRIBUTIONS

J.L. and S.K. wrote Manuscript; J.L., A.F.S, and P.M.L. designed Research; J.L., A.F.S, K.A.D., C.I.M., J.M.L, J.M., and P.M.L. performed research; J.L., S.K., A.F.S, and P.M.L. analyzed Data; T.J.M. contributed new reagents/Analytical Tools.

Keywords

1-(2'-deoxy-2'-fluoro-β-D-arabinofuranosyl) uracil (FAU); Parent-metabolite population pharmacokinetic model; Positron emission tomography (PET); Thymidylate synthase; Tumor pharmacokinetics

INTRODUCTION

The knowledge of drug exposure and kinetics in tumor and normal tissues can provide a mechanistic understanding of the target modulation and off-target effect and help predicting the efficacy and toxicity of a chemotherapeutic agent. However, conventional pharmacokinetic (PK) studies in early phase clinical trials are usually performed by measuring drug concentrations in the system (plasma) as a function of time after drug administration. While plasma PK is critical to the selection of the most appropriate route of administration and dosing regimen, it reveals little information on tumor and normal tissue PK. Tumor biopsies could be obtained in some cases, but the procedure is invasive and sparse biopsy samples are generally collected, which does not allow characterization of the drug tissue kinetics. Advances in modern imaging techniques have led to a noninvasive approach that can be used to obtain PK data from deep tissues[1, 2].

Positron emission tomography (PET) is a noninvasive, quantitative, and highly sensitive dynamic imaging modality that provides an idea tool in evaluating tissue pharmacology of radiolabeled drugs[1, 2]. Given its high temporal and spatial resolution as well as tomographic imaging with excellent quantitative accuracy, dynamic PET imaging allows measurement of radioactivity – time course of a drug candidate radiolabeled with a positron emitting radionuclide in blood and different tissues. However, one major technical drawback associated with dynamic PET imaging is the short follow-up time, restricted by the radioactive half-life of the radionuclide. For example, in PET studies with ^{18}F-labeled drugs, the 110 min radioactive half-life of ^{18}F restricts the dynamic PET imaging times up to a few hours. Hence, although it may provide important information on the drug distribution and disposition in the early kinetic phase, dynamic PET study has limited value in characterizing late-phase kinetics for drugs with a biological half-life longer than the radioactive half-life of the tracer[3]. Therefore, combining conventional plasma PK study and dynamic PET assessment is a logical strategy that allows the acquirement of long-term plasma PK data along with tissue kinetic information from the same patients. When a tracer dose (< 100 μg) of radiolabeled drug is co-administered with a therapeutic dose of unlabeled drug, dynamic PET allows accurate determination of radioactivity concentrations in tumor and normal tissues. As the radiolabeled and unlabeled drugs are chemically identical, they share identical tissue distribution and disposition. Thus, tissue concentrations of the unlabeled drug can be derived from the tracer radioactivity concentrations. Nevertheless, PET measures total radioactivity concentrations in the region of interest regardless of the molecules the radiolabel belongs to. This limitation could be overcome by an appropriate PK model that makes it possible to distinguish the parent drug signal from signals of metabolites[4].

Here, we present a model-based approach to integrating conventional plasma PK and dynamic PET studies to characterize the plasma and tumor PK of 1-(2'-deoxy-2'-fluoro-β-D-arabinofuranosyl) uracil (FAU), a first-in-class investigational anticancer agent. FAU is a pyrimidine nucleoside that acts as a suicide prodrug. FAU has been shown to be readily transported into cells and converted by intracellular thymidine kinase (TK) to its monophosphate, 1-(2-deoxy-2-fluoro-β-D-arabinofuranosyl) uracil monophosphate that is further methylated by intracellular thymidylate synthase (TS) to form 1-(2-deoxy-2-fluoro-β-D-arabinofuranosyl) 5-methyluracil monophosphate (FMAU)[5]. Then, the methylated product (FMAU) is incorporated into DNA causing cell death[5]. Greater DNA incorporation of FAU metabolites in cell lines with high TS activity resulted in increased cytotoxicity compared to cell lines with lower TS activity[5]. In light of the essential role of TS in DNA biosynthesis, inhibition of this enzyme using chemotherapeutic agents such as 5-fluorouracil (5-FU) and capecitabine (orally bioavailable 5-FU prodrug) is an important antitumor strategy. However, tumors with high TS expression/activity can develop resistance to TS inhibitors[6, 7]. FAU, taking advantage of high TS activity in the tumor as a mechanism of activation, may provide an effective treatment for patients whose tumors overexpress TS and are resistant to TS inhibitor-based therapy. FAU has been evaluated for the safety, PK, and potential antitumor activity in a phase I clinical trial, where we combined dynamic PET assessment using ^{18}F-FAU as the tracer and conventional plasma PK evaluation of therapeutic FAU to better understand the disposition and bioactivation of FAU in cancer patients.

In this study, we compiled FAU and FMAU plasma concentration data determined by liquid chromatography coupled with tandem mass spectrometry (LC-MS/MS) in the conventional PK study as well as the total FAU plus FMAU tissue concentration data derived from the dynamic PET assessment. By simultaneously fitting all the data, we developed a parent-metabolite population model that simultaneously characterized the plasma, normal and tumor tissue PK of the parent drug (FAU) and its active metabolite (FMAU).

METHODS

Patients and Treatment

The protocol was approved by the Wayne State University Institutional Review Board (IRB #: 090807M1F). A written informed consent was obtained from each patient. All procedures were in accordance with the ethical standards of the responsible committee on human experimentation or with the Helsinki Declaration of 1975 (as revised in 1983). Twelve patients with histologically or cytologically confirmed diagnosis of solid tumors that are metastatic or refractory to standard treatment were enrolled in the phase I study of FAU (NCI study #7916). Additional eligibility criteria included age above 18 years, an Eastern Cooperative Oncology Group performance status of 2 or less, adequate marrow function (leukocyte count ≥ 3×10^9/L, absolute neutrophil count ≥ 1.5×10^9/L, platelet count ≥ 100×10^9/L), adequate liver and kidney functions (total bilirubin ≤ 2 mg/dL, aspartate aminotransferase and alanine aminotransferase ≤ 2.5 times the institution upper limit of normal, calculated creatinine clearance ≥ 60 mL/min/1.73 m^2), and no chemotherapy within 4 weeks prior to the enrollment.

FAU was provided by the National Cancer Institute Division of Cancer Treatment and Diagnosis (Bethesda, MD) as injection solution (25 mg/mL FAU in 0.45% sodium chloride solution, USP). The first two patients (001 and 002) were treated with FAU at the dose of 800 and 1600 mg/m^2/day, respectively, as a 1-hour intravenous infusion daily for 5 consecutive days of a 28-day cycle. These two patients experienced Grade 3 neuropathy. Because of the toxicity and based on the preliminary PK data, the FAU dosing regimen was adjusted for the rest of patients. Patients 003 – 012 were treated with FAU at 50 or 100 mg/m^2 administered as a 1-hour intravenous infusion weekly for 4 weeks (on day 1, 8, 15, and 22) of a 28-day cycle.

Conventional Plasma PK Study

Plasma PK of FAU was evaluated in all 12 patients. Serial blood sampling was obtained at pre-infusion, 1, 1.25, 1.5, 2, 3, 5, 8 h, and 24 h after the start of infusion on day 1 (for all patients) and day 5 (for Patient 001 and 002 receiving FAU 800 or 1600 mg/m^2 daily for 5 days) or day 22 (for Patients 003 – 012 receiving FAU 50 or 100 mg/m^2 weekly for 4 weeks). Blood samples were collected in EDTA tubes, placed on ice, and processed within 1 hour of collection. Plasma was separated by centrifugation at 1500 g at 4°C for 10 minutes, and stored at −80 °C until analysis. The plasma concentrations of FAU and FMAU were determined using a validated liquid chromatography coupled with tandem mass spectrometry (LC-MS/MS) method[8].

PET Study

PET procedure—PET study was performed using ^{18}F-FAU as the tracer. ^{18}F-FAU was synthesized using 2-O-[(trifluoromethyl)sulfonyl]-1,3,5-tri-O-benzoyl-α-D-ribofuranose as the substrate for the initial kryptofix[2.2.2]-facilitated nucleophilic fluorination with fluoride-18, as described previously[9]. Radiopharmaceuticals were quality checked to ensure sterility and apyrogenicity. The chemical and radiochemical purity was > 95% with specific activity > 2.8 × 10^{13} Bq/mol.

Two PET scans were performed in each individual patient. The first PET scan was performed within 14 days before the treatment with therapeutic FAU, and the second was performed at a median time of 1.5 h after the intravenous infusion of FAU (50 – 1600 mg/m^2) on Day 1 of Cycle 1. For each scan, a microdose of ^{18}F-FAU was administered intravenously through a peripheral venous cannula over ~ 1 min, followed by dynamic PET scanning for 1 h and serial venous blood sampling. Dynamic PET scans were performed on a whole body PET scanner ECAT EXACT/HR (Siemens, Knoxville, TN). The emission scans were measured dynamically for a total acquisition time of 1 h. The measured sonograms were corrected for attenuation, detector efficiency (scatter, random, dead time), and detector nonuniformity, and reconstructed into tomographic images. PET imaging data were then calibrated to microcurie per milliliter (μCi/mL). Regions of interest (ROI) representing the liver and tumor were manually defined on the PET images with the aid of computed tomography films. The radioactivity per unit volume (μCi/mL) for each ROI was derived for each time frame to obtain radioactivity versus time curves. Throughout the scans, serial venous blood samples were collected from an intravenous catheter that was different from the one used for the tracer injection. Plasma was separated from blood samples by

centrifugation (1500 g, 4°C, 10 minutes). The plasma radioactivity associated with the unchanged ^{18}F-FAU and its potential metabolites were separated using a high-performance liquid chromatography (HPLC) method, and radioactivity concentrations (μCi/mL) were determined by a Packard Cobra II Auto-Gamma Counter Model D5005, as described previously[10].

PET Data for PK Modeling—Given the fact that the radiolabeled and unlabeled drugs are chemically identical, the plasma/tissue concentrations of the unlabeled drug can be calculated from the tracer radioactivity concentrations when the tracer is administered concomitantly with a therapeutic dose of the unlabeled drug, using Eq. 1[11].

$$\text{Unlabeled Drug Concentration}\left(\frac{\mu g}{\text{mL}}\right)=\text{SUV}\times\text{Therapeutic Dose per Body Weight}\ (\mu g/g) \quad (1)$$

where the standardized uptake value (SUV) is defined as plasma/tissue radioactivity concentration (μCi/mL) at a particular time point decay corrected to the time of injection and normalized to the injected radioactivity dose per body weight (μCi/g).

Since PET measured the total concentration of ^{18}F (consisting of ^{18}F-FAU and ^{18}F-FMAU) in a region of interest, the total tissue concentrations of FAU plus FMAU in the liver and tumor following concomitant intravenous injection of the therapeutic FAU (50, 100, 800, or 1600 mg/m^2) and tracer ^{18}F-FAU in individual patients could be constructed based on PET-measured radioactivity – time curves, using Eq. 1. Pooled data including LC-MS/MS-determined FAU and FMAU plasma concentrations following 1-h intravenous infusion of FAU (at 50, 100, 800, and 1600 mg/m^2), PET-derived FAU plasma concentrations after intravenous injection of FAU (at 50, 100, 800, and 1600 mg/m^2), as well as PET-derived total FAU plus FMAU liver and tumor concentrations after intravenous injection of FAU (at 50, 100, 800, and 1600 mg/m^2), were simultaneously fitted to a parent-metabolite population PK model, as described in the next section.

Population PK Modeling and Simulation

Model structure—Both two- and three-compartment models with first-order elimination from the central compartment were tested to fit the plasma concentration – time profiles of FAU and ^{18}F-FAU. Based on the model selection criteria as described below, three- and two-compartment models were selected for FAU and ^{18}F-FAU, respectively, as their final models. For the comparison of PK profiles between FAU and ^{18}F-FAU, the models were parameterized in both micro-constants (e.g., CL and V) and macro-constants (e.g., A, B, C, α, β, γ).

Several parent-metabolite models were tested to simultaneously describe FAU and FMAU plasma and tissue PK profiles. The initial model was a three-compartment model where the disposition of FAU and FMAU occurred in 3 compartments representing the plasma, liver,

and tumor, and the conversion of FAU to FMAU was characterized by first-order kinetics. Then the complexity of the initial model was increased stepwise by replacing first-order kinetics with Michaelis-Menten kinetics to characterize the conversion of FAU to FMAU and by adding another compartment to describe the disposition of FAU and FMAU in other peripheral tissues. Based on the selection criteria outlined below, a complex parent-metabolite compartment model (as shown in Figure 2) was selected as the final model, where the disposition of FAU and FMAU occurred in 4 compartments representing the plasma, liver, tumor, and other peripheral tissues, and the conversion of FAU to FMAU was characterized by Michaelis-Menten kinetics (Eq. 2) in tissue compartments (including tumor, liver and other peripheral tissues).

$$R=\frac{V_{\max} \times C}{K_m+C} \quad (2)$$

where R is the metabolic conversion rate; V_{max} is the maximum conversion rate; K_m is the substrate (FAU) concentration at which half-maximum conversion rate is achieved; and C represents the substrate (FAU) concentration. It is assumed that the metabolism of FAU to FMAU in different tissues exhibits different V_{max} (representing different enzyme abundance) but a same K_m value (representing same enzyme affinity to FAU). As TK and TS are mainly expressed in tissues (tumor and normal tissues) but negligibly in blood, the conversion of FAU to FMAU is assumed to occur in tissue compartments only.

Parameter estimation—Population PK analyses were performed using the nonlinear mixed effects (population) modeling approach with the MONOLIX software Version 4.3.2 (http://software.monolix.org). The R software version 3.1.2 (www.R-project.org) was used for graphical visualization and diagnosis. All concentration data were log-transformed in the data file. Population PK parameters, variability, and residual error were assessed in the model. The variability (including interindividual and inter-occasional variability) on individual PK parameter was modeled as an exponential function. Notably, the interindividual and inter-occasional variabilities couldn't be differentiated due to the relatively small sample size and the complexity of the model. Thus, the estimated variability represents the combined interindividual and inter-occasional variability. Residual error was modeled with a combination method, including an additive and a proportional error component. Parameter estimation was performed by using the Stochastic Approximation of the Expectation Maximization (SAEM) algorithm in combination with the Markov Chain Monte Carlo (MCMC) method, as implemented in MONOLIX, where parameters were estimated by computing the maximum likelihood estimator of the parameters without any approximation of the model and standard error for the maximum likelihood estimator. Individual PK parameters were obtained by posterior Bayesian estimation. Below the lower limit of quantitation (BLQ) data were considered as left censored data and were taken into account in the MONOLIX estimation using the left censored lower limit of quantitation. The MONOLIX structure model code for the final parent-metabolite model is presented in Supplementary Appendix 1.

Model selection—Model selection aims at identifying a model that best fits the observed data with the smallest possible dimension. Model selection was guided by a number of model evaluation criteria, including Akaike Information Criterion (AIC), objective function value (OFV; −2log likelihood), precision of estimates (relative standard error of the estimate), and goodness-of-fit plots. The likelihood ratio test was used to compare between hierarchical models. Assuming that the OFV is χ^2 distributed, a decrease in OFV of 3.84 between hierarchical models with one parameter differing is considered as statistically significant difference ($P < 0.05$). AIC was used to compare between non-hierarchical models. AIC is calculated as (−2LL) + 2 × p, where −2LL is the OFV and p is the number of parameters. Candidate models with lower AIC were selected over those with higher AIC. In addition, the following criteria were also considered when selecting a model: 1) better precision of estimates (reduction of the relative standard errors of estimates); 2) minimization of interindividual variability; and 3) no prediction bias as visualized from goodness-of-fit plots.

Model evaluation—The final parent-metabolite model was further assessed using a visual predictive check[12], where a parametric bootstrap resampling was used to simulate 1,000 replicates of the observed dataset based on the original study design and final parameter estimates. In addition, identifiability of the model parameters was assessed using a previously reported method[13]. The diagnostic procedure (i.e., convergence assessment) available in MONOLIX was used. First, 20 intervals of individual parameters were constructed based on the final parameter estimates. Specifically, the lower and upper bounds of the intervals were set as multiplying the final estimate by 0.6 and 1.65, respectively, which are the same as subtracting and adding 0.5 to the final estimate in log-scale. Then, 50 runs were performed by using the set of initial values randomly selected from the 20 intervals. If the 95% confidence intervals of a parameter estimate from 50 runs are overlapped with the 95% confidence intervals of the final parameter, this parameter was considered as statistically identifiable.

Simulations—To illustrate the potential utility of the model for selecting optimal dosing regimen, FAU and FMAU concentration – time profiles in the plasma, tumor and normal tissues were simulated in a typical individual (with population PK parameters) following 1-h intravenous infusion of FAU (1600 mg/m^2) with 4 different treatment schedules (i.e., daily for 5 days of a 28-day cycle, 3 day on/4 day off for 4 weeks, weekly for 4 weeks, and biweekly for 4 weeks). In addition, to demonstrate the potential utility of the model for predicting the clinical response to FAU, the plasma and tumor concentration – time profiles of FAU and FMAU were simulated in a typical individual whose tumor has varying TS catalytic activity, i.e., V_{max2}/K_m = 1.6 (population median value), 0.16, or 16 h^{-1}, following daily FAU treatment (1600 mg/m^2) for 5 days of a 28-day cycle.

RESULTS

Comparison of Plasma PK between therapeutic FAU and tracer ^{18}F-FAU

Multiple-dose plasma concentration – time profiles of FAU following 1-h intravenous infusion daily for 5 days (at the dose of 800 or 1600 mg/m^2) or weekly for 4 weeks (at the

dose of 50 or 100 mg/m^2) (Figure 2A) were well described by a linear three-compartment model, which was characterized by a fast and slow disposition phase (with a half-life of 0.9 and 6.9 h, respectively) and a terminal elimination phase (with a half-life of 7.7 h). Goodness-of-fit plots are shown in Supplementary Figure S-1A. Population plasma PK parameters of FAU estimated from the models parameterized in micro or macro constants are summarized in Table 1.

Single-dose plasma radioactivity concentration – time profiles of ^{18}F-FAU in individual patients following an intravenous injection of the tracer ^{18}F-FAU concomitantly with the administration of therapeutic FAU were not significantly different from those following the injection of the tracer alone (Figure 2C), suggesting that the presence of therapeutic concentrations of FAU in the body did not influence the distribution and disposition of the tracer. These data confirmed the linear (dose-independent) PK of FAU, at least at the tested dose levels (50 – 1600 mg/m^2). The plasma radioactivity – time profiles of ^{18}F-FAU from all patients were adequately described by a linear two-compartment model, characterized by a rapid distribution and slow disposition phase (with a half-life of 0.03 and 5.3 h, respectively). Goodness-of-fit plots are shown in Supplementary Figure S-1B. Population PK parameters of ^{18}F-FAU are summarized in Table 1.

The comparison of PK parameters between FAU and ^{18}F-FAU revealed that the tracer kinetics well mirrored the early-phase kinetic profile of the therapeutic FAU, as indicated by an excellent concordance between FAU and ^{18}F-FAU parameters (i.e., V1, V2, CL12, CL, K12, K21 and K10) that characterized the drug distribution and disposition in the central compartment (V1) and rapidly equilibrating compartment (V2) (Table 1). However, limited by the short radioactive half-life of ^{18}F (110 min), the tracer ^{18}F-FAU could not capture the distribution and disposition kinetics of FAU in the slowly equilibrating compartment (V3) and during the terminal elimination phase.

Parent-metabolite PK model simultaneously describing plasma and tissue PK of FAU and FMAU

The plasma levels of FMAU were approximately 3 orders of magnitude lower than those of FAU in individual patients following 1-h intravenous infusion of FAU (Figure 2A and 2B). Interestingly, FMAU was accumulated in the system (plasma) after either daily or weekly FAU treatment (Figure 2B). For example, in patients who received daily FAU infusion (800 or 1600 mg/m^2) for 5 consecutive days, FMAU systemic exposure (i.e., C_{max}, and AUC) increased by ~10 fold on day 5 compared to that on day 1, and FMAU trough plasma levels consistently increased from treatment days 2 to 5 (Figure 2B). The accumulation of FMAU in the system was also noted in the patients receiving weekly FAU infusion for 4 weeks at lower dose levels (50 and 100 mg/m^2), as indicated by the observation that FMAU plasma concentrations were below the lower limit of quantitation (< 0.001 μg/mL) on day 1, while becoming measurable on day 22 (Figure 2B).

A parent-metabolite population PK model (Figure 1) was developed to simultaneously fit LC-MS/MS-determined FAU and FMAU plasma concentrations as well as PET-derived total FAU plus FMAU liver and tumor tissue concentrations (Figure 2E). The model adequately described the observed data, as suggested by goodness-of-fit plots (Supplementary Figure

S-2) and visual predictive check (Supplementary Figure S-3). Model-predicted and LC-MS/MS-determined FAU and FMAU plasma concentration – time profiles in two representative individual patients receiving 5-day daily and 4-week weekly FAU treatment are shown in Figure 3A1 and 3A2, respectively. The model-predicted and PET-derived total FAU plus FMAU concentration – time profiles in the tumor and liver following a single-dose intravenous injection of FAU in these two patients are shown in Figures 3B1/2 and 3C1/2, respectively. Notably, the parent-metabolite model enabled the PET-derived total FAU plus FMAU tissue concentrations to be distinguished into the parent drug (FAU) and metabolite (FMAU) components (Figures 3B1/2 and 3C1/2). Thus, the model not only well described the observed FMAU accumulation in plasma (Figures 3A1 and 3A2), but also predicted accumulation of FMAU in the tumor (Figures 3B1 and 3B2), following chronic daily or weekly FAU treatment.

Typical population PK parameters estimated from the parent-metabolite model are summarized in Table 2. Following intravenous administration, FAU rapidly distributed from the systemic circulation (Plasma; V1) to the liver (V2) and other peripheral tissues (V4) (at a distribution rate constant of 28.6 and 50.7 h^{-1}, respectively), while relatively slowly distributing to the tumor (V3) (at a distribution rate constant of 12.0 h^{-1}). FAU underwent metabolic conversion to FMAU in the tumor, liver, and other peripheral tissues, with an intrinsic clearance (V_{max}/K_m) of 1.6, 2.5×10^{-4}, and 8.4×10^{-4} L/h, respectively (Table 2), suggesting that the tumor exhibited a significantly higher catalytic activity (V_{max}/K_m) for conversion of FAU to FMAU compared to normal tissues. Once it was formed, FMAU was released from the tumor, liver, and other peripheral tissues to the systemic circulation (plasma), at a rate constant of 3.6×10^{-4}, 11.5, and 2.5×10^{-3} h^{-1}, respectively (Table 2). Concurrently, FMAU was eliminated from the plasma at an elimination rate constant of 7.6 h^{-1}.

Model identifiability

There are two types of identifiability in nonlinear models in general, including mathematical identifiability and statistical identifiability. Mathematical identifiability also referred to as structural or deterministic identifiability is the identifiability of model parameters from noise-free data. Statistical identifiability, also termed as numerical identifiability, is the identifiability of parameters estimated from noise data[14–16]. The mathematical identifiability mostly is not a challenge in PK modeling because a PK model is developed by the use of the ordinary differential equations that have solid theoretical and mathematical foundations. The major challenge in identifiability of PK modeling predominantly occurs from the statistical identifiability because of the paucity of samples and high residual variability. Several methods have been published to diagnose the statistical identifiability of PK modeling[13–19]. In these methods, numerous runs with different initial values are performed, and then convergence to different solutions can indicate a lack of identifiability[13–19]. Using this approach, the statistical identifiability of the parent-metabolite model was assessed. As shown in Supplementary Figure S-4, the 95% confidence intervals of each individual parameter estimated from 50 runs with different initial values were overlapped with the 95% confidence intervals of the final parameter, indicating the identifiability of the model parameters.

It should be noted that the diagnostic method used here does not guarantee that all parameter estimates have unique solutions in the entire domain (i.e., globally identifiable), but it ensures that parameter estimates have unique solutions in the neighborhood of the final estimates (i.e., locally identifiable). Thus, there may be a possibility that some parameter estimates had a finite number of alternate solutions in the entire domain. Very large standard errors of estimation may indicate some issues in the parameterization. Given the sparse observed FMAU concentration data, it was not surprising that several PK parameters for describing FMAU kinetics (i.e., V8, CL58, and V_{max3}) exhibited a relatively large standard error of estimation (> 50%) (Table 2). These parameters may not be reliably estimated. Nevertheless, it has been well recognized that a trade-off between model complexity and parameter identifiability may be needed based on available clinical data[13]. Despite the limitation noted here, the developed parent-metabolite model provided reasonable, clinical meaningful parameter estimates to describe the plasma and tissue PK profiles of FAU and FMAU.

Predictions from the parent-metabolite model

With the developed parent-metabolite model, the plasma and tumor/normal tissue concentration – time profiles of FAU and FMAU were predicted in a typical individual treated with 4 different FAU treatment schedules (i.e., 3 day on/4 day off for 4 weeks, daily for 5 days of a 28-day cycle, weekly for 4 weeks, and biweekly for 4 weeks) (Figure 4). Predicted drug exposure parameters, including steady state $C_{ss,max}$ and $C_{ss,min}$ and 28-day cumulative $AUC_{0–672h}$, are summarized in Table 3. While there was no apparent difference in FAU plasma or tumor/normal tissue steady-state levels (i.e., $C_{ss,max}$ and $C_{ss,min}$) following different treatment schedules, higher cumulative plasma and tissue exposure (i.e., $AUC_{0–672h}$) to FAU were achieved following the more intensive dosing regimen than the less intensive regimen (Figure 4 and Table 3). For example, FAU plasma $AUC_{0–672h}$ was ~ 6-fold higher following 3 day on/4 day off schedule than following biweekly schedule (Table 3). Notably, 5-day daily and 4-week weekly schedules resulted in similar plasma/tissue exposure to FAU (including steady-state levels and cumulative $AUC_{0–672h}$) (Table 3).

Compared to FAU, the impact of treatment schedules on FMAU plasma and tissue exposure was more pronounced. In general, the more intensive dosing regimen resulted in higher FMAU steady-state level and higher cumulative exposure ($AUC_{0–672h}$) in plasma and tumor/normal tissues than the less intensive regimen (Figure 4 and Table 3). FMAU cumulative tumor exposure ($AUC_{0–672h}$) was increased by 83% following 5-day daily treatment schedule, compared to 4-week weekly treatment (Table 3). With further increasing dosing intensity (e.g., following 4-week 3 day on/4 day off schedule), FMAU $AUC_{0–672h}$ was increased moderately in the tumor (by 54%) as compared to that following 5-day daily schedule (Table 3). These data suggested that 5-day daily schedule may be the optimal dosing regimen to achieve adequate tumor exposure. However, the first two patients experienced grade 3 neuropathy when being treated with FAU at the dose of 800 mg and 1600 mg daily for 5 days. While the exact mechanism underlying neuropathy remained unknown, a more conservative dosing regimen (i.e., 4-week weekly treatment at 50 and 100 mg/m^2) was applied to the subsequent patients. It should be noted that although the conservative regimen produced a favorable safety profile (data not shown here), it might

result in sub-therapeutic FMAU concentrations in tumors. This could be a potential reason for the lack of clinical efficacy in the present phase I study.

In addition, the developed parent-metabolite model was used to predict the bioactivation of FAU and retention of FMAU in tumors with varying catalytic activity (i.e., V_{max2}/K_m) for the conversion of FAU to FMAU. Supplementary Figure S-5 shows the simulated FAU and FMAU concentration – time profiles in the plasma, tumor, liver, and other tissues following daily FAU infusion (1600 mg/m^2) for 5 days of a 28-day cycle in a typical individual with the V_{max2}/K_m value varying 10 fold relative to the population median value. Table 4 summarizes the predicted plasma and tissue exposure parameters of FAU and FMAU, including $AUC_{0–2h}$ (as a measure of early retention), $AUC_{0–24h}$, and $AUC_{0–672h}$ (as a measure of cumulative exposure). In general, with increasing tumor catalytic activity (V_{max2}/K_m), FMAU plasma and tumor/normal tissue exposure was increased, while FAU exposure was decreased (Table 4). The impact of V_{max2}/K_m on FMAU exposure was more significant than that on FAU exposure. These data collectively suggested that the tumoral catalytic activity towards the conversion of FAU to FMAU was an important determinant of the tumor exposure to FMAU.

DISCUSSION

The process of integrating dynamic PET assessment into early phase clinical trials to obtain information on drug distribution to normal and tumor tissues have been applied in the development of a number of anticancer drugs such as 5-FU, BCNU (an alkylating agent specific for brain tissue), DACA (a topoisomerase I/II inhibitor), and SMT487 (a somatostatin analogue)[20–23]. However, the major barriers to the utility of dynamic PET for plasma and tissue PK evaluation are the short follow up time of PET and its inability to distinguish the radiolabeled parent drug and metabolites. This study, for the first time to our best knowledge, presents a pharmacometric modeling approach to overcome these barriers by simultaneously modeling dynamic PET tissue data and long-term conventional plasma PK data. This modeling approach enables separation of the PET-derived total tissue concentrations into the parent drug (FAU) and metabolite (FMAU) components, thus allowing simultaneous characterization of the plasma, normal and tumor tissue PK of FUA and FMAU. The developed parent-metabolite model not only complements previous knowledge on the disposition of FAU and ^{18}F-FAU, but also provides further quantitative, mechanistic insights into the bioactivation of FAU and retention of FMAU in normal and tumor tissues.

First, the parent-metabolite model suggests that the tumor exhibits > 100 fold higher catalytic activity (V_{max}/K_m) for the conversion of FAU to FMAU than normal tissues (Table 2), implying that the bioactivation of FAU occurs predominantly in the tumor, but is negligible in normal tissues. This could be attributable, for a large part, to the overexpression of intratumoral TS, a rate-limiting determinant for the conversion of FAU to FMAU. While FAU must undergo multiple steps, including transport across the cell membrane, phosphorylation by TK and methylation by TS, prior to its incorporation into DNA, TS activity has been proven to be the critical, rate-limiting determinant for incorporation of FAU into cellular DNA as FMAU[5]. TS is an E2F1-regulated enzyme that is essential for DNA

synthesis and repair, with the physiological function of converting deoxyuridine monophosphate (dUMP) to deoxythymidine monophosphate (dTMP)[24]. TS protein and mRNA levels are elevated in many human cancers, and high TS levels have been correlated with poor prognosis in patients with colorectal, breast, cervical, bladder, kidney, and non-small cell lung cancers[24–30]. It has been demonstrated that ectopic expression of catalytically active human TS is sufficient to induce a transformed phenotype in mammalian cells *in vitro* and *in vivo*, indicating an oncogene-like role of TS in tumorigenesis[31]. In addition, cells can acquire resistance to TS inhibitors (e.g., 5-FU) through TS gene amplification[32–34]. Tumors with high TS gene expression are generally non-responsive to 5-FU based therapies[7, 35, 36]. Although the data regarding the intratumoral TS mRNA/protein levels are not available in the present study, elevated intratumoral TS expression/activity would be expected in the majority, if not all, of the patients enrolled in this phase I trial, whose tumors are advanced and refractory to standard treatments (including 5-FU). The preferential activation of FAU in tumors as indicated by the parent-metabolite model provides quantitative evidence supporting the concept of using the high catalytic activity of intratumoral TS to activate deoxyuridine prodrugs (such as FAU) to form toxic metabolites that can be incorporated into DNA and act as suicide inhibitors of cell growth[37].

Second, the parent-metabolite model suggests that the toxic metabolite FMAU is slowly released from the tumor to systemic circulation (with a half-life of 57 days) (Table 2) and it is accumulated in tumors after either 5-day daily or 4-week weekly FAU treatment (Figure 3), indicating that FMAU is trapped in tumors once it is formed. These findings are consistent with the observations from preclinical *in vivo* tissue distribution studies using radiolabeled tracers with a long radioactive half-life[385]. In the study with ^{14}C-FAU (radioactivity half-life, 5730 y) in a human tumor xenograft mouse model, ^{14}C-FAU rapidly distributed throughout the body in a generally nonspecific manner immediately after the injection (≤ 2 h), whereas differential and preferential accumulation of radioactivity in the tumor was magnified over time[38]. Specifically, at 2 h after the intravenous injection of ^{14}C-FAU, similar amounts of radioactivity were detected in all tissues examined; whereas at 24 h after the injection, only tumor tissues contained appreciable amounts of radioactivity, and further examination of purified genomic DNA from tumor and all other tissues indicated that radioactivity was accumulated in tumor DNA only but not in all other tissues[38]. Similar pattern was also observed for tissue distributions of ^{3}H-FAU (radioactive half-life, 12.3 y) in mice bearing colorectal cancer xenografts[5]. These results collectively suggest that the radioactivity recovered from tumor tissues at later times (e.g., 24 h) reflects the incorporation of FMAU (converted from FAU) into tumor DNA because the DNA-incorporated drug (FMAU) persists while the un-incorporated drug (FAU) is cleared out of tissues over time.

It should be mentioned that ^{18}F-FAU has been evaluated for its potential as a PET probe in dogs and humans[10, 39]. ^{18}F-FAU evenly distributed to most organs in dogs and humans, and in contrast to ^{18}F labeled thymidine and its analogs, bone marrow had less retention of ^{18}F-FAU than non-proliferating tissues[10, 39]. In patients with breast cancer, tumors had ~ 2-fold higher retention of ^{18}F-FAU than normal tissues[39]. Based on these preliminary data, it has been speculated that PET measurement of ^{18}F-FAU tumor retention may provide important predictive information to determine which patients are likely to respond to therapeutic FAU.

However, findings from the modeling and simulations provide strong evidence against this speculation, as follows: First, the parent-metabolite model suggests that FAU is rapidly cleared from the tumor, but FMAU is trapped in the tumor. As a consequence, the observed tumor radioactivity (total ^{18}F-FAU plus ^{18}F-FMAU) is dominantly attributable to ^{18}F-FAU at early times (e.g., ≤ 2 h), but to ^{18}F-FMAU at later times (Figures 2B1 and 2B2). However, an extension of dynamic PET imaging of ^{18}F to longer times (i.e., > 2 h) is hampered due to the short radioactive half-life (~ 110 min). Thus, PET-measured early-time tumor retention of ^{18}F is not a reliable marker for the tumor exposure to FMAU, the cytotoxic metabolite exerting antitumor activity. Second, the parent-metabolite model enables separation of the PET-derived total tissue concentrations into the parent drug (FAU) and metabolite (FMAU) components, it is therefore possible to predict the tumor and normal tissue exposure to FMAU. Given the determinant role of TS catalytic activity for the conversion of FAU to FMAU, tumors with higher catalytic activity (i.e., V_{max2}/K_m) would be expected to retain more FMAU than those with lower activity. As expected, simulations demonstrate that individuals with higher tumor V_{max2}/K_m exhibit higher FMAU tumor exposure (including early exposure $AUC_{0–2h}$, $AUC_{0–24h}$, and cumulative $AUC_{0–672h}$) than those with lower V_{max2}/K_m (Table 4 and Supplementary Figure S-5). On the contrary, the simulated $AUC_{0–2h}$ of total FAU plus FMAU in the tumor, which represents the PET-measured intratumoral radioactivity of ^{18}F at early times (up to 2 h), is similar across tumors with varying V_{max2}/K_m (Table 4), suggesting that the PET-measured early time intratumoral radioactivity cannot truly reflect the differential incorporation of FAU into DNA as FMAU in tumors with varying catalytic activity. These data further indicate that the use of PET measurement of ^{18}F-FAU tumor retention has little value in guiding selection of patients for FAU treatment.

Despite the lack of efficacy data to validate the model, the developed parent-metabolite model has a potential utility not only for predicting tumor responsiveness but also for guiding the selection of dosing regimen, as demonstrated by simulations. The apparent limitation for the model presented is the relatively small sample size used in its development. Although the model's identifiability has been demonstrated (Supplementary Figure S-4), the relative standard error of estimation for several PK parameters related to FMAU kinetics and formation (e.g., V8, CL58, and V_{max3}) are over 50% (Table 2), given the sparse observed FMAU data (with ~2/3 of observed FMAU plasma concentrations below the lower limit of quantitation). Another limitation is that the model doses not differentiate the inter-individual PK variability and inter-occasion variability (i.e., variability between LC-MS/MS determined data and PET-derived data). These limitations may hinder the clinical applicability of the model for accurate prediction of tumor responsiveness to FAU. Regardless, the developed parent-metabolite model provides clinical meaningful, quantitative insights into the bioactivation of FAU and accumulation of the active metabolite FMAU in the tumor.

Although the development of FAU was discontinued because of a patient death caused by potential drug-related delayed liver injury, our study may have important implications for drug development in general for two reasons. First, it demonstrates the feasibility and advantage of integrating long-term conventional plasma PK study and dynamic PET assessment into early-phase clinical trials. Second, it illustrates the necessity and utility of

PK modeling approaches to separate PET-derived tissue concentrations into the parent drug and metabolite components, thus allowing quantitatively assess drug distribution and metabolism (in particular bioactivation) in tumor and normal tissues. This makes it possible to not only choose optimal treatment schedules but also select most appropriate patient population for further development.

Supplementary Material

Refer to Web version on PubMed Central for supplementary material.

Acknowledgments

This study was supported by the United States Public Health Service Cancer Center Support Grant P30 CA022453 and the National Institute of Health Grant U01 CA062487. We particularly thank the patients enrolled in the study.

References

1. Klimas MT. Positron emission tomography and drug discovery: contributions to the understanding of pharmacokinetics, mechanism of action and disease state characterization. Molecular imaging and biology : MIB : the official publication of the Academy of Molecular Imaging. 2002; 4(5):311–337. [PubMed: 14537107]
2. Boss DS, Olmos RV, Sinaasappel M, Beijnen JH, Schellens JH. Application of PET/CT in the development of novel anticancer drugs. The oncologist. 2008; 13(1):25–38. [PubMed: 18245010]
3. Saleem A, Aboagye EO, Matthews JC, Price PM. Plasma pharmacokinetic evaluation of cytotoxic agents radiolabelled with positron emitting radioisotopes. Cancer chemotherapy and pharmacology. 2008; 61(5):865–873. [PubMed: 17639391]
4. Kissel J, Brix G, Bellemann ME, et al. Pharmacokinetic analysis of 5-[18F]fluorouracil tissue concentrations measured with positron emission tomography in patients with liver metastases from colorectal adenocarcinoma. Cancer research. 1997; 57(16):3415–3423. [PubMed: 9270007]
5. Eiseman JL, Brown-Proctor C, Kinahan PE, et al. Distribution of 1-(2-deoxy-2-fluoro-beta-D-arabinofuranosyl) uracil in mice bearing colorectal cancer xenografts: rationale for therapeutic use and as a positron emission tomography probe for thymidylate synthase. Clinical cancer research : an official journal of the American Association for Cancer Research. 2004; 10(19):6669–6676. [PubMed: 15475457]
6. Johnston PG, Drake JC, Trepel J, Allegra CJ. Immunological quantitation of thymidylate synthase using the monoclonal antibody TS 106 in 5-fluorouracil-sensitive and -resistant human cancer cell lines. Cancer Res. 1992; 52(16):4306–4312. [PubMed: 1643628]
7. Salonga D, Danenberg KD, Johnson M, et al. Colorectal tumors responding to 5-fluorouracil have low gene expression levels of dihydropyrimidine dehydrogenase, thymidylate synthase, and thymidine phosphorylase. Clin Cancer Res. 2000; 6(4):1322–1327. [PubMed: 10778957]
8. Wiegand R, Wu J, Shields AF, Lorusso P, Li J. Simultaneous determination of 1-(2'-deoxy-2'-fluoro-beta-D-arabinofuranosyl) uracil (FAU) and 1-(2'-deoxy-2'-fluoro-beta-D-arabinofuranosyl) 5-methyluracil (FMAU) in human plasma by liquid chromatography/tandem mass spectrometry. Journal of chromatography B, Analytical technologies in the biomedical and life sciences. 2012; 891–892:64–70.
9. Mangner TJ, Klecker RW, Anderson L, Shields AF. Synthesis of 2'-deoxy-2'-[18F]fluoro-beta-D-arabinofuranosyl nucleosides, [18F]FAU, [18F]FMAU, [18F]FBAU and [18F]FIAU, as potential PET agents for imaging cellular proliferation. Synthesis of [18F]labelled FAU, FMAU, FBAU, FIAU. Nuclear medicine and biology. 2003; 30(3):215–224. [PubMed: 12745012]
10. Sun H, Collins JM, Mangner TJ, Muzik O, Shields AF. Imaging [18F]FAU [1-(2'-deoxy-2'-fluoro-beta-D-arabinofuranosyl) uracil] in dogs. Nuclear medicine and biology. 2003; 30(1):25–30. [PubMed: 12493539]

11. Bergstrom M, Grahnen A, Langstrom B. Positron emission tomography microdosing: a new concept with application in tracer and early clinical drug development. European journal of clinical pharmacology. 2003; 59(5–6):357–366. [PubMed: 12937873]
12. Post TM, Freijer JI, Ploeger BA, Danhof M. Extensions to the visual predictive check to facilitate model performance evaluation. Journal of pharmacokinetics and pharmacodynamics. 2008; 35(2): 185–202. [PubMed: 18197467]
13. Lavielle M, Samson A, Karina Fermin A, Mentre F. Maximum likelihood estimation of long-term HIV dynamic models and antiviral response. Biometrics. 2011; 67(1):250–259. [PubMed: 20486926]
14. Godfrey KR, Fitch WR. The Deterministic Identifiability of Nonlinear Pharmacokinetic Models. J Pharmacokinet Biop. 1984; 12(2):177–191.
15. Kim S, Li L. A Switching Markov Chain Monte Carlo Method for Statistical Identifiability of Nonlinear Pharmacokinetics Models. Stat Sinica. 2012; 22(3):1199–1215.
16. Kim S, Li L. Statistical identifiability and convergence evaluation for nonlinear pharmacokinetic models with particle swarm optimization. Comput Meth Prog Bio. 2014; 113(2):413–432.
17. Hengl S, Kreutz C, Timmer J, Maiwald T. Data-based identifiability analysis of non-linear dynamical models. Bioinformatics. 2007; 23(19):2612–2618. [PubMed: 17660526]
18. Miao HY, Dykes C, Demeter LM, Wu HL. Differential Equation Modeling of HIV Viral Fitness Experiments: Model Identification, Model Selection, and Multimodel Inference. Biometrics. 2009; 65(1):292–300. [PubMed: 18510656]
19. Lavielle M, Samson A, Fermin AK, Mentre F. Maximum Likelihood Estimation of Long-Term HIV Dynamic Models and Antiviral Response. Biometrics. 2011; 67(1):250–259. [PubMed: 20486926]
20. Moehler M, Dimitrakopoulou-Strauss A, Gutzler F, Raeth U, Strauss LG, Stremmel W. 18F-labeled fluorouracil positron emission tomography and the prognoses of colorectal carcinoma patients with metastases to the liver treated with 5-fluorouracil. Cancer. 1998; 83(2):245–253. [PubMed: 9669806]
21. Tyler JL, Yamamoto YL, Diksic M, et al. Pharmacokinetics of superselective intra-arterial and intravenous [11C]BCNU evaluated by PET. Journal of nuclear medicine : official publication, Society of Nuclear Medicine. 1986; 27(6):775–780.
22. Saleem A, Harte RJ, Matthews JC, et al. Pharmacokinetic evaluation of N-[2-(dimethylamino)ethyl]acridine-4-carboxamide in patients by positron emission tomography. Journal of clinical oncology : official journal of the American Society of Clinical Oncology. 2001; 19(5):1421–1429. [PubMed: 11230487]
23. Propper DJ, de Bono J, Saleem A, et al. Use of positron emission tomography in pharmacokinetic studies to investigate therapeutic advantage in a phase I study of 120-hour intravenous infusion XR5000. Journal of clinical oncology : official journal of the American Society of Clinical Oncology. 2003; 21(2):203–210. [PubMed: 12525511]
24. Johnston PG, Lenz HJ, Leichman CG, et al. Thymidylate synthase gene and protein expression correlate and are associated with response to 5-fluorouracil in human colorectal and gastric tumors. Cancer Res. 1995; 55(7):1407–1412. [PubMed: 7882343]
25. Leichman CG. Predictive and prognostic markers in gastrointestinal cancers. Curr Opin Oncol. 2001; 13(4):291–299. [PubMed: 11429488]
26. Mizutani Y, Wada H, Yoshida O, et al. Significance of thymidylate synthase activity in renal cell carcinoma. Clin Cancer Res. 2003; 9(4):1453–1460. [PubMed: 12684419]
27. Nomura T, Nakagawa M, Fujita Y, Hanada T, Mimata H, Nomura Y. Clinical significance of thymidylate synthase expression in bladder cancer. Int J Urol. 2002; 9(7):368–376. [PubMed: 12165018]
28. Pestalozzi BC, Peterson HF, Gelber RD, et al. Prognostic importance of thymidylate synthase expression in early breast cancer. J Clin Oncol. 1997; 15(5):1923–1931. [PubMed: 9164203]
29. Shintani Y, Ohta M, Hirabayashi H, et al. New prognostic indicator for non-small-cell lung cancer, quantitation of thymidylate synthase by real-time reverse transcription polymerase chain reaction. Int J Cancer. 2003; 104(6):790–795. [PubMed: 12640689]

30. Suzuki M, Tsukagoshi S, Saga Y, Ohwada M, Sato I. Enhanced expression of thymidylate synthase may be of prognostic importance in advanced cervical cancer. Oncology. 1999; 57(1):50–54. [PubMed: 10394125]

31. Rahman L, Voeller D, Rahman M, et al. Thymidylate synthase as an oncogene: a novel role for an essential DNA synthesis enzyme. Cancer Cell. 2004; 5(4):341–351. [PubMed: 15093541]

32. Berger SH, Jenh CH, Johnson LF, Berger FG. Thymidylate synthase overproduction and gene amplification in fluorodeoxyuridine-resistant human cells. Mol Pharmacol. 1985; 28(5):461–467. [PubMed: 2932632]

33. Danenberg KD, Danenberg PV. Activity of thymidylate synthetase and its inhibition by 5-fluorouracil in highly enzyme-overproducing cells resistant to 10-propargyl-5,8-dideazafolate. Mol Pharmacol. 1989; 36(2):219–223. [PubMed: 2528057]

34. Spears CP, Gustavsson BG, Berne M, Frosing R, Bernstein L, Hayes AA. Mechanisms of innate resistance to thymidylate synthase inhibition after 5-fluorouracil. Cancer Res. 1988; 48(20):5894–5900. [PubMed: 3167844]

35. Leichman CG, Lenz HJ, Leichman L, et al. Quantitation of intratumoral thymidylate synthase expression predicts for disseminated colorectal cancer response and resistance to protracted-infusion fluorouracil and weekly leucovorin. J Clin Oncol. 1997; 15(10):3223–3229. [PubMed: 9336359]

36. Leichman L, Lenz HJ, Leichman CG, et al. Quantitation of intratumoral thymidylate synthase expression predicts for resistance to protracted infusion of 5-fluorouracil and weekly leucovorin in disseminated colorectal cancers: preliminary report from an ongoing trial. Eur J Cancer. 1995; 31A(7–8):1306–1310. [PubMed: 7577041]

37. Collins JM, Klecker RW, Katki AG. Suicide prodrugs activated by thymidylate synthase: rationale for treatment and noninvasive imaging of tumors with deoxyuridine analogues. Clin Cancer Res. 1999; 5(8):1976–1981. [PubMed: 10473074]

38. Wang H, Oliver P, Nan L, et al. Radiolabeled 2'-fluorodeoxyuracil-beta-D-arabinofuranoside (FAU) and 2'-fluoro-5-methyldeoxyuracil-beta -D-arabinofuranoside (FMAU) as tumor-imaging agents in mice. Cancer chemotherapy and pharmacology. 2002; 49(5):419–424. [PubMed: 11976837]

39. Sun H, Collins JM, Mangner TJ, Muzik O, Shields AF. Imaging the pharmacokinetics of [F-18]FAU in patients with tumors: PET studies. Cancer chemotherapy and pharmacology. 2006; 57(3):343–348. [PubMed: 16001172]

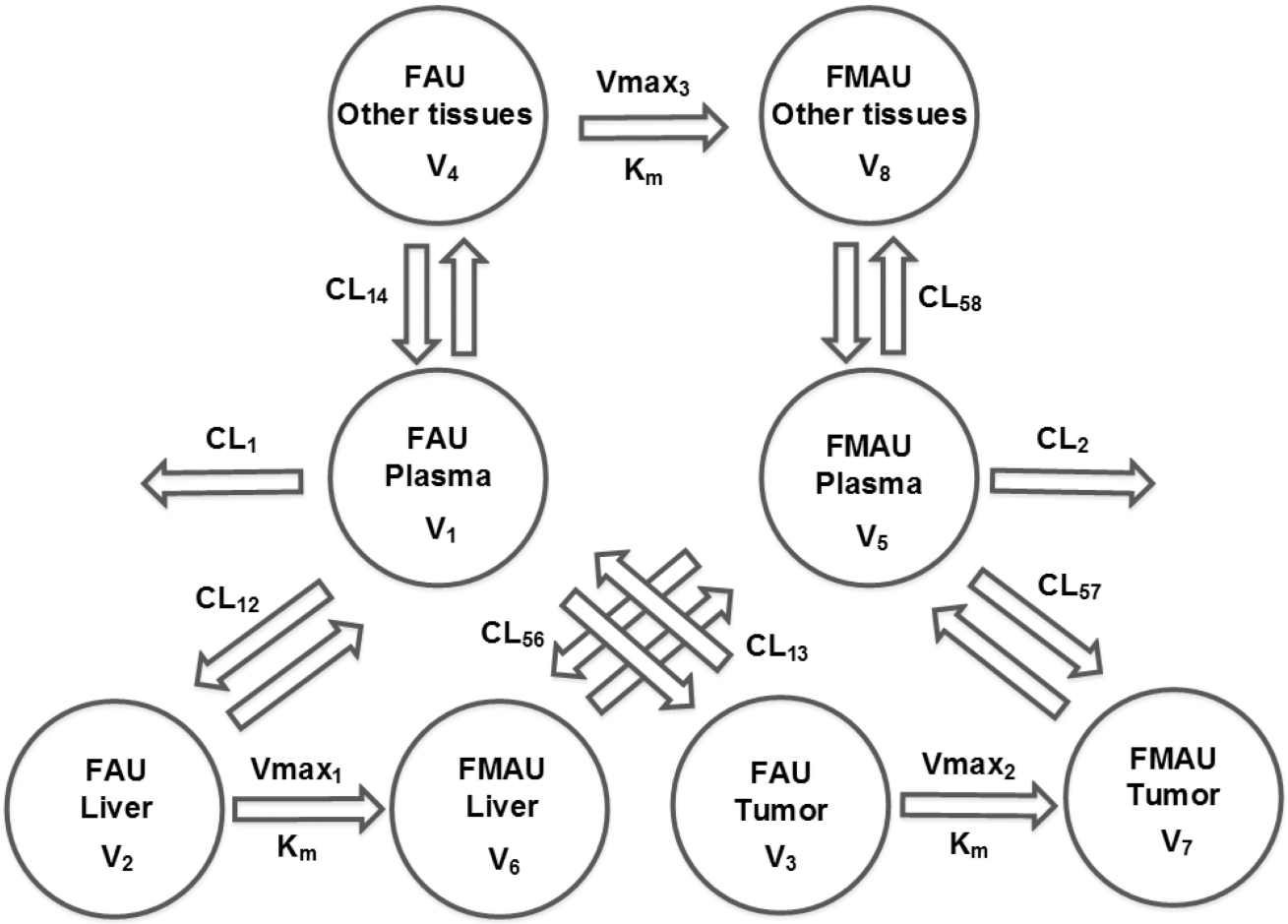

Figure 1.

Schematic illustration of the parent–metabolite pharmacokinetic model that simultaneously characterizes the plasma and tissue pharmacokinetics of FAU and its active metabolite FMAU.

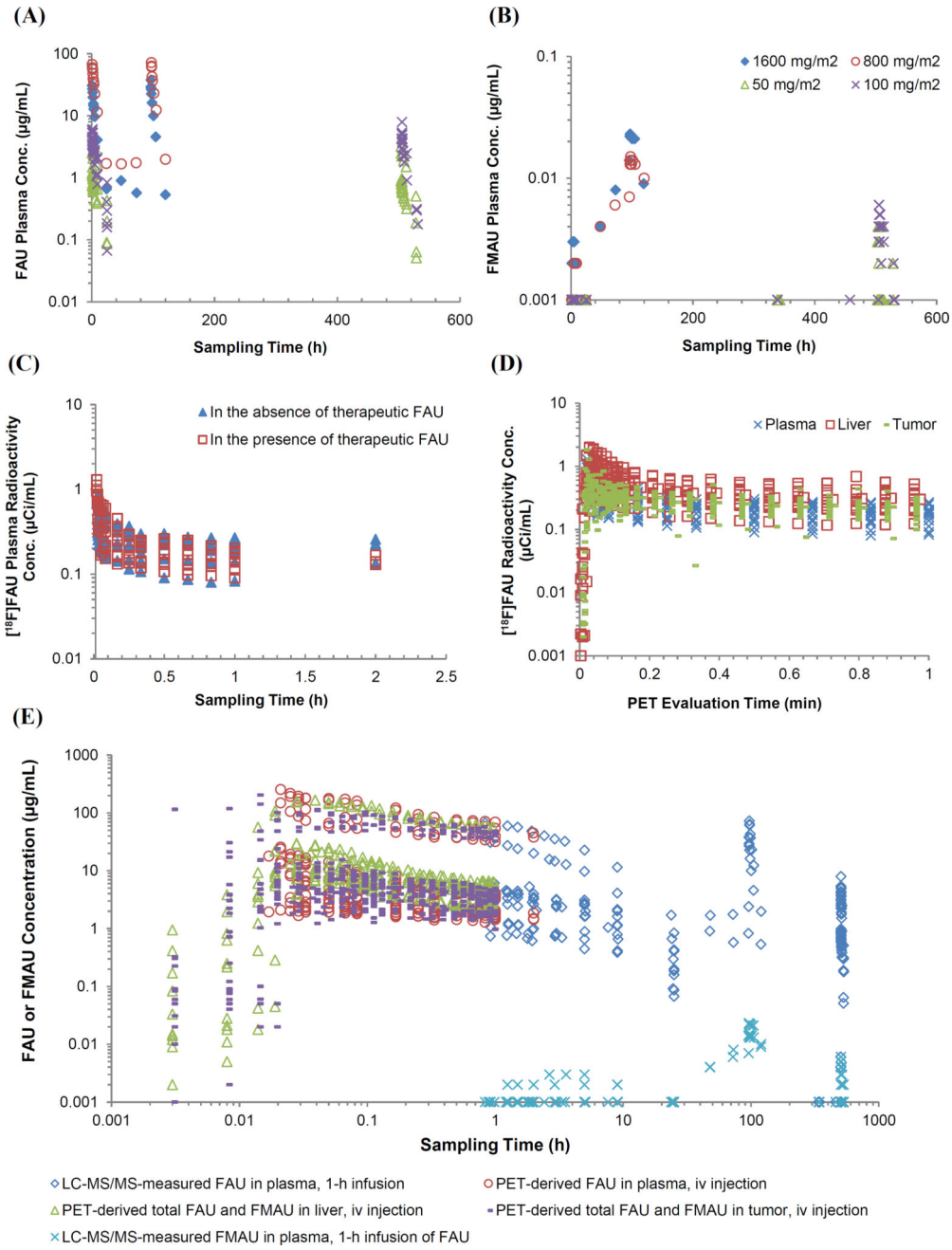

Figure 2.

Observed concentration data obtained from conventional pharmacokinetic study and dynamic PET assessment. (**A and B**) Observed multiple-dose plasma concentration – time profiles of FAU and FMAU in individual patients treated with a 1-h intravenous infusion of FAU daily (800 or 1600 mg/m^2) for 5 days or weekly (50 or 100 mg/m^2) for 4 weekly. (**C**) Observed plasma radioactivity concentration – time profiles of ^{18}F-FAU in individual patients receiving an intravenous injection of the tracer prior to and during intravenous infusion of the therapeutic FAU. (**D**) Observed plasma radioactivity concentration – time profiles of ^{18}F-FAU as well as radioactivity concentration – time profiles of ^{18}F

(including ^{18}F-FAU and ^{18}F-FMAU) in the liver and tumor in individual patients receiving an intravenous injection of the tracer prior to and during intravenous infusion of the therapeutic FAU. (E) Pooled data acquired from conventional pharmacokinetic study and dynamic PET assessment, including 1) plasma concentrations of FAU and FMAU following 1-h intravenous infusion of FAU (at 50, 100, 800, and 1600 mg/m^2) determined by LC-MS/MS; and 2) plasma concentrations of FAU as well as liver and tumor concentrations of total FAU plus FMAU after intravenous injection of FAU (at 50, 100, 800, and 1600 mg/m^2) calculated based on the SUVs from dynamic PET study.

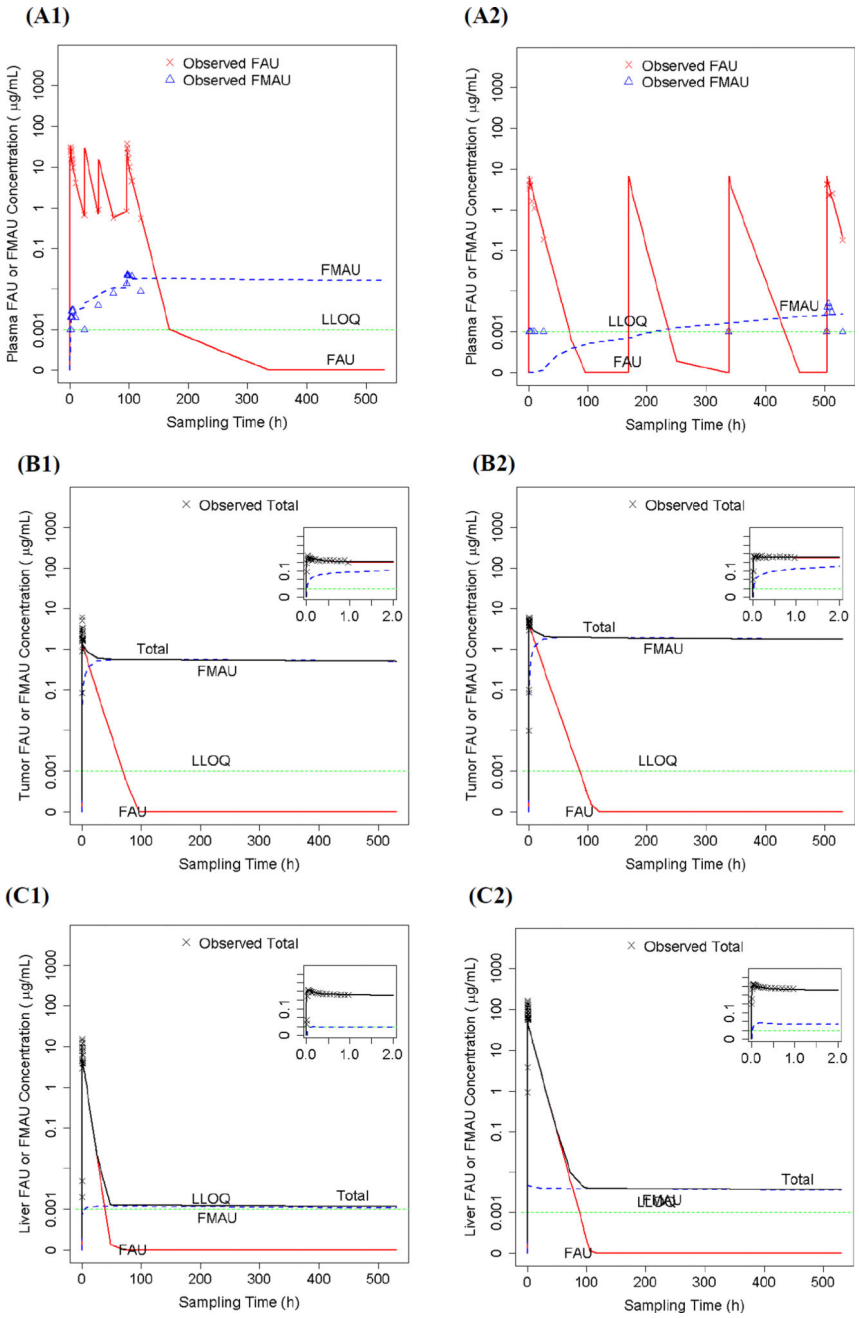

Figure 3.

(**A1 and A2**) LC-MS/MS-determined and parent-metabolite model-predicted plasma concentration – time profiles of FAU and its metabolite FMAU in two representative patients treated with 1-h intravenous infusion of FAU either daily (1600 mg/m^2) for 5 days of a 28-day cycle (**A1**) or weekly (100 mg/m^2) for 4 weeks of a 28-day cycle (**A2**). (**B1 and B2**) PET-derived and parent – metabolite model-predicted tumor concentration – time profiles of FAU/FMAU in the same two representative patients receiving a single intravenous injection of FAU at the dose of 1600 mg/m^2 (**B1**) or 100 mg/m^2 (**B2**). (**C1 and C2**) PET-derived and parent-metabolite model-predicted liver concentration – time profiles of FAU/FMAU in the

same two representative patients receiving a single intravenous injection of FAU at the dose of 1600 mg/m^2 (**C1**) or 100 mg/m^2 (**C2**).

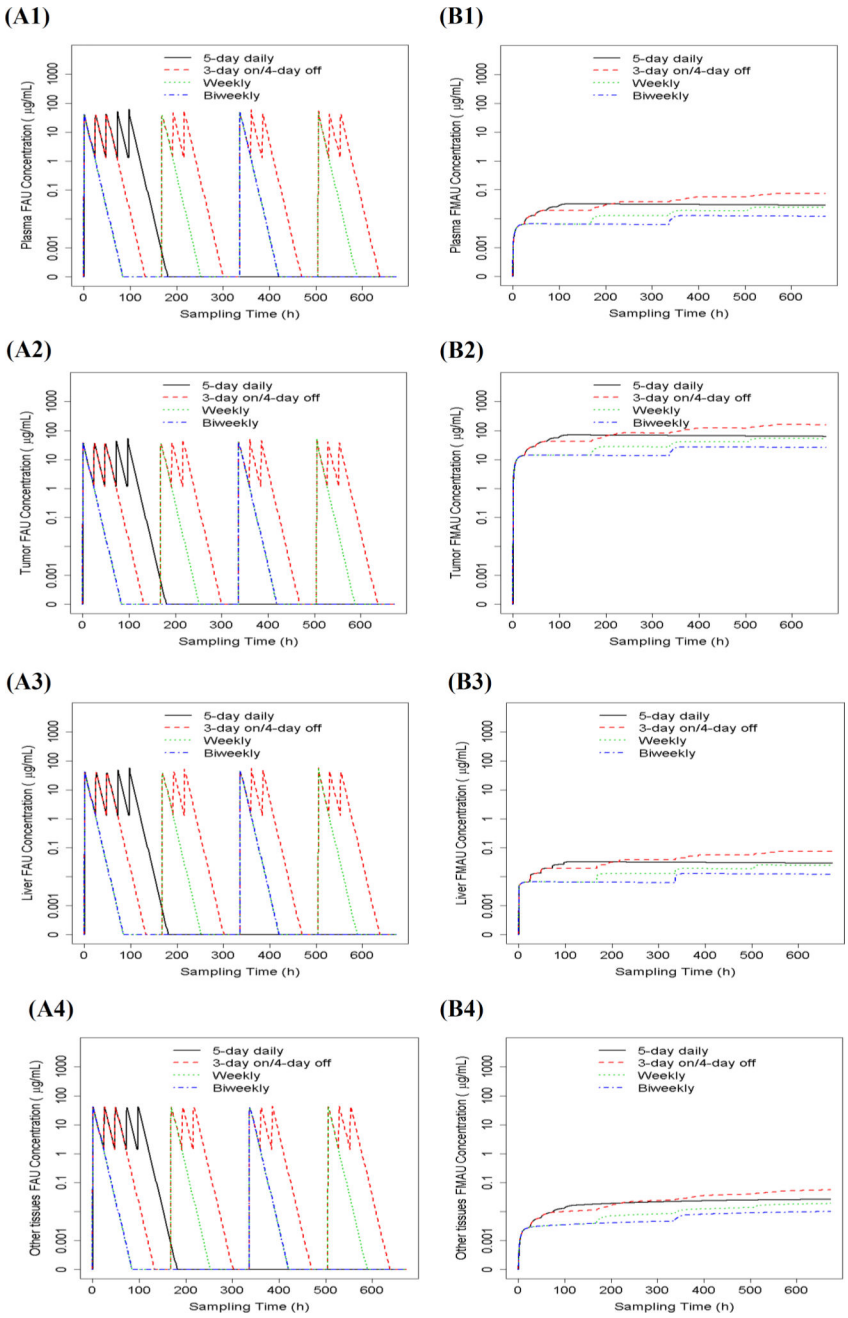

Figure 4.

Parent-metabolite model-predicted concentration – time profiles of FAU (**A1–A4**) and FMAU (**B1–B4**) in the plasma, tumor, liver, and other peripheral tissues in a typical individual treated with 1-h intravenous infusion of FAU (1600 mg/m^2) at 4 different dosing regimens (i.e., daily for 5 days of a 28-day cycle, 3 day on/4 day off for 4 weeks, weekly for 4 weeks, and biweekly for 4 weeks).

Table 1

Plasma pharmacokinetic parameters of therapeutic FAU and tracer ^{18}F-FAU in cancer patients

	FAU[a]		^{18}F-FAU[b]	
Parameter	**Population estimate (%RSE)**	**IIV (%) (%RSE)**	**Population estimate (%RSE)**	**IIV (%) (%RSE)**
Macro Model				
α (h^{-1})	0.81 (18)	17 (42)	24.07 (−)	72 (14)
β (h^{-1})	0.10 (1)	33 (9)	0.13 (5)	108 (28)
γ (h^{-1})	0.09 (54)	-	-	-
A (mg/L)	0.008 (0.2)	95 (25)	0.07 (1)	42 (12)
B (mg/L)	0.01 (0.2)	38 (9)	0.02 (0)	24 (5)
C (mg/L)	0.0002 (0.02)	111 (87)	-	-
Additive residual error	0.18 (1)	17 (42)	0.12 (1)	
OFV	276.1		−613.7	
Micro Model				
V1 (L)	9.3 (41)	139.1 (21)	10.3 (4)	9.9 (39)
V2 (L)	28.8 (6)	13.0 (39)	30.5 (8)	31.5 (20)
V3 (L)	20.5 (53)	167.5 (23)	-	-
CL12 (L/h)	223.4 (12)	13.4 (82)	173.1 (20)	76.0 (19)
CL13 (L/h)	5.0 (8)	6.6 (219)	-	-
CL (L/h)	5.6 (17)	56.0 (21)	5.8 (22)	75.1 (23)
K12[c] (h^{-1})	24.0		16.8	
K21[c] (h^{-1})	7.8		5.7	
K13[c] (h^{-1})	0.54		-	
K31[c] (h^{-1})	0.24		-	
K10[c] (h^{-1})	0.60		0.56	
Additive residual error[d]	0.24 (7)		0.20 (11)	
Proportional residual error[e]	0.05 (10)		0.06 (22)	
OFV	9.3		−112.3	

[a]Parameters of FAU were estimated by simultaneously fitting FAU multiple-dose plasma concentration – time profiles from 12 patients receiving 1-h intravenous infusion of FAU daily (800 or 1600 mg/m^2) or weekly (50 or 100 mg/m^2) to a three-compartment linear model.

[b]Parameters of ^{18}F-FAU were estimated by simultaneously fitting ^{18}F-FAU plasma radioactivity concentration – time profiles from 12 patients receiving an intravenous injection of a tracer dose prior to and during FAU infusion to a two-compartment linear model.

[c]Calculated from population estimates of CL and V, using equations: K12 = CL12/V1; K21 = CL12/V2; K13 = CL13/V1; K31 = CL13/V3; K10 = CL/V1

[d]Additive component (a) in the residue error model: $y = f + (a + b \cdot f) \cdot e$.

[e]Proportional component (b) in the residue error model: $y = f + (a + b \cdot f) \cdot e$

Abbreviations: V1, volume of distribution in the central compartment; V2 and V3, volume of distribution in the peripheral compartments; CL12 and CL13, inter-compartment clearance; CL, systemic clearance; K12 and K21, distribution rate constant from V1 to V2 and from V2 to V1, respectively; K13 and K31, distribution rate constant from V1 to V3 and from V3 to V1, respectively; K10, elimination rate constant from the

central compartment; IIV, inter-individual variability; OFV, objective function value (−2 times log transformed likelihood); RSE, relative standard error of estimation.

Table 2

Population pharmacokinetic parameters of FAU and FMAU, estimated from the parent-metabolite pharmacokinetic model[a]

	Population estimate (%RSE)	Variability (%)[b] (%RSE)
FAU		
V1 (L)	1.1 (45)	300.0 (10)
V2 (L)	2.7 (5)	1.9 (665)
V3 (L)	1.3 (37)	209.0 (14)
V4 (L)	26.6 (7)	29.9 (20)
CL12 (L/h)	31.5 (25)	119.0 (16)
CL13 (L/h)	13.2 (31)	163.0 (16)
CL14 (L/h)	55.8 (19)	95.0 (15)
CL1 (L/h)	3.8 (15)	63.1 (18)
FMAU		
V5 (L)	1.6 (35)	142.0 (19)
V6 (L)	0.2 (39)	77.2 (49)
V7 (L)	27.6 (22)	29.6 (81)
V8 (L)	40.2 (100)	102.0 (136)
CL56 (L/h)	2.3 (22)	37.0 (48)
CL57 (L/h)	0.01 (25)	39.5 (67)
CL58 (L/h)	0.1 (65)	70.9 (133)
CL2 (L/h)	12.2 (24)	23.5 (151)
Conversion of FAU to FMAU		
K_m (mg/L)	119 (18)	20.3 (149)
V_{max1} (mg/h)	0.03 (29)	36.3 (62)
V_{max2} (mg/h)	191 (27)	115.0 (−)
V_{max3} (mg/h)	0.1 (70)	151.0 (42)
Residual Errors[c]		
Additive (plasma)	0.02 (33)	
Proportional (plasma)	0.1 (5)	
Additive (liver)	0.4 (6)	
Proportional (liver)	0.3 (4)	
Additive (tumor)	0.2 (33)	
Proportional (tumor)	0.3 (8)	
Proportional (metabolite)	0.5 (−)	
OFV	4770.4	

[a] Parameters were estimated by simultaneously fitting LC-MS/MS-determined FAU and FMAU plasma concentrations as well as PET-derived liver and tumor concentrations of FAU plus FMAU in 12 patients.

[b] Combined inter-individual variability and inter-occasion variability (i.e., variability between LC-MS/MS determined data and PET-derived data).

[c] Residue error model: $y = f + (a + b \cdot f) \cdot e$, where f is the parametric function of the pharmacokinetic compartment model, a is an additive component, b is a proportional component, and e is the residual error.

Abbreviations: V, volume of distribution; CL12, CL13, CL14, CL56, CL57, and CL58, inter-compartment clearance; CL1 and CL2, systemic clearance of FAU and FMAU, respectively; OFV, objective function value (−2 times log transformed likelihood); RSE, relative standard error of estimation.

Table 3

Parent-metabolite model predicted plasma and tumor/normal tissue exposure to FAU and FMAU following 4 different treatment schedules with 1-h intravenous infusion of FAU (1600 mg/m^2) in a typical individual with population pharmacokinetic parameters

		4 day on/3 day off for 4 weeks	Daily for 5 days of a 28-day cycle	Weekly for 4 weeks	Biweekly for 4 weeks
FAU	**Plasma**				
	$C_{ss,max}$ (μg/ml)	59.51	61.42	52.83	48.72
	$C_{ss,min}$ (μg/ml)	BLQ	1.28	BLQ	BLQ
	AUC_{0-672h} (μg/ml*h)	3673	1538	1219	603
	AUC_{0-2h} (μg/ml*h)	27	27	27	27
	Tumor				
	$C_{ss,max}$ (μg/ml)	53.52	53.33	53.52	41.18
	$C_{ss,min}$ (μg/ml)	BLQ	1.16	BLQ	BLQ
	AUC_{0-672h} (μg/ml*h)	3354	1398	1118	551
	AUC_{0-2h} (μg/ml*h)	26	26	26	26
	Liver				
	$C_{ss,max}$ (μg/ml)	58.25	58.09	58.25	45.18
	$C_{ss,min}$ (μg/ml)	BLQ	1.3	BLQ	BLQ
	AUC_{0-672h} (μg/ml*h)	3698	1541	1233	607
	AUC_{0-2h} (μg/ml*h)	28	28	28	28
	Other Tissues				
	$C_{ss,max}$ (μg/ml)	44.18	42.44	42.44	42.44
	$C_{ss,min}$ (μg/ml)	BLQ	1.38	BLQ	BLQ
	AUC_{0-672h} (μg/ml*h)	3753	1561	1250	623
	AUC_{0-2h} (μg/ml*h)	29	29	29	29
FMAU	**Plasma**				
	$C_{ss,max}$ (μg/ml)	0.07	0.03	0.03	0.01
	$C_{ss,min}$ (μg/ml)	0.06	0.02	0.02	0.01

	4 day on/3 day off for 4 weeks	Daily for 5 days of a 28-day cycle	Weekly for 4 weeks	Biweekly for 4 weeks
AUC_{0-672h} (μg/ml*h)	30	19	10	6
AUC_{0-2h} (μg/ml*h)	0.001	0.001	0.001	0.001
Tumor				
$C_{ss,max}$ (μg/ml)	160.07	69.74	53.75	27.32
$C_{ss,min}$ (μg/ml)	119.98	40.3	39.34	12.12
AUC_{0-672h} (μg/ml*h)	63052	41057	22356	13377
AUC_{0-2h} (μg/ml*h)	1	1	1	1
Liver				
$C_{ss,max}$ (μg/ml)	0.08	0.03	0.03	0.01
$C_{ss,min}$ (μg/ml)	0.06	0.02	0.02	0.01
AUC_{0-672h} (μg/ml*h)	30	19	11	6
AUC_{0-2h} (μg/ml*h)	0.003	0.003	0.003	0.003
Other Tissues				
$C_{ss,max}$ (μg/ml)	0.06	0.03	0.02	0.01
$C_{ss,min}$ (μg/ml)	0.04	0.01	0.01	0
AUC_{0-672h} (μg/ml*h)	19	14	7	4
AUC_{0-2h} (μg/ml*h)	< 0.001	< 0.001	< 0.001	< 0.001

BLQ, below the lower limit of quantitation (FAU concentration < 0.001 μg/mL)

Table 4

Parent-metabolite model predicted plasma, tumor, liver, and other tissue exposure to FAU and FMAU in a typical individual whose tumor has low, median, and high catalytic activity (i.e., V_{max2}/K_m value of 0.16, 1.6, and 16 h-1, respectively) for the conversion of FAU to FMAU, following daily 1-h infusion of FAU (1600 mg/m2) for 5 days of a 28-day cycle.

V_{max2}/K_m (h^{-1})	AUC (mg/L*h)	FAU				FMAU			
		Plasma	Tumor	Liver	Other tissues	Plasma	Tumor	Liver	Other tissues
0.16	AUC_{0-2h}	28	29	29	29	0.001	0.2	0.003	0.0003
	AUC_{0-24h}	356	358	361	377	0.02	30	0.1	0.1
	AUC_{0-672h}	1983	1968	1987	2007	3	5599	3	7
1.6	AUC_{0-2h}	27	26	28	29	0.001	1	0.003	0.0003
	AUC_{0-24h}	283	261	288	304	0.1	242	0.1	0.05
	AUC_{0-672h}	1538	1398	1541	1561	19	41057	19	14
16	AUC_{0-2h}	21	10	22	24	0.004	8	0.01	0.0003
	AUC_{0-24h}	122	59	127	143	0.4	770	0.4	0.03
	AUC_{0-672h}	694	329	697	714	51	109153	51	26